ACS APPLIED MATERIALS & INTERFACES

Research Article

www.acsami.org

Optoelectrochemical Biorecognition by Optically Transparent Highly Conductive Graphene-Modified Fluorine-Doped Tin Oxide Substrates

F. Lamberti,[†,‡,§] L. Brigo,[†,§] M. Favaro,[∥] C. Luni,[†,‡,§] A. Zoso,[†,‡] M. Cattelan,[∥] S. Agnoli,[∥] G. Brusatin,[†,§] G. Granozzi,[∥] M. Giomo,[†,§] and N. Elvassore*[,†,‡,§]

[†]Department of Industrial Engineering, University of Padova, Via Marzolo 9, 35131 Padova, Italy

[‡]Venetian Institute of Molecular Medicine (VIMM), Via Orus 2, 35129 Padova, Italy

[§]National Interuniversity Consortium of Materials Science and Technology (INSTM), Via Giuseppe Giusti, 9, 50121 Firenze, Italy

[∥]Department of Chemical Sciences, University of Padova, Via Marzolo 1, 35131 Padova, Italy

Supporting Information

ABSTRACT: Both optical and electrochemical graphene-based sensors have gone through rapid development, reaching high sensitivity at low cost and with fast response time. However, the complex validating biochemical operations, needed for their consistent use, currently limits their effective application. We propose an integration strategy for optoelectrochemical detection that overcomes previous limitations of these sensors used separately. We develop an optoelectrochemical sensor for aptamer-mediated protein detection based on few-layer graphene immobilization on selectively modified fluorine-doped tin oxide (FTO) substrates. Our results show that the electrochemical properties of graphene-modified FTO samples are suitable for complex biological detection due to the stability and inertness of the engineered electrodic interface. In addition, few-layer immobilization of graphene sheets through electrostatic linkage with an electrochemically grafted FTO surface allows obtaining an optically accessible and highly conductive platform. As a proof of concept, we used insulin as the target molecule to reveal in solution. Because of its transparency and low sampling volume (a few microliters), our sensing unit can be easily integrated in lab-on-a-chip cell culture systems for effectively monitoring subnanomolar concentrations of proteins relevant for biomedical applications.

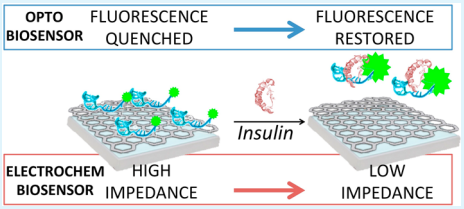

KEYWORDS: *insulin detection, optoelectrochemical analysis, FRET, electrochemically reduced graphene oxide, FTO, TCO*

1. INTRODUCTION

Optical and electrochemical biosensor performance has been extensively optimized both by continuously reducing the detection limits and by increasing the sensitivity and specificity of the measurements.[1,2] During the past few years scientists have focused their attention on developing new biosensing interfaces for small-molecule and single-molecule detection systems.[3,4] In this wide context, graphene-based biosensors are emerging as relevant sensing platforms. Optical and electrochemical biosensors based on graphene sheets are increasingly acquiring scientific and medical interest.[5]

The functional principle of these optical biosensors is based on the interference of the radiative emission of a dye-labeled probe (typically nucleic acids) bound to a graphene surface by $\pi-\pi$ interactions,[6] resulting in the so-called superquenching effect.[7,8] Aptamers, increasingly used as probes, are synthetic low molecular weight nucleic acids whose sequence is selected to have a high affinity toward a specific chemical species.[9] They easily attach on graphene by electrostatic interactions and are modified without difficulty to be labeled with a fluorophore. When biological targets present in solution detach the adsorbed aptamers from the graphene surface, the radiative emission is restored, resulting in sensitive and specific biosensors. This significant property of graphene has been used to create highly sensitive optical biosensors for biological targets, as reported for dsDNA,[10] thrombin,[11] insulin,[12] ATP,[8] ochratoxicin A,[13] and other biomolecules.[14−17] However, these systems require rather complex sample preparation and medium dilution to collect spectra using laboratory conventional detection equipment.[7,8,18−20] Moreover, signal amplification is often required because of the low concentration of probe released from the surface to reduce the limit of detection of these optical systems.[12]

On the other hand, graphene-based electrochemical biosensors exploit the relevant catalytic properties of graphene.[21] Several such biosensors have already been reported.[22−25] Production of graphene thin films requires complex and expensive chemical vapor deposition (CVD) processes[26,27] and also presents limitations as for the type of starting substrate. Thus, graphene-based sensors are usually engineered starting from graphene oxide (GO), which has the great advantage of being water soluble.[28−30] GO, because of oxygen defects in the basal plane, is an insulating material, and a reductive step is required to achieve an elevated electron mobility within the

Received: October 9, 2014
Accepted: December 1, 2014
Published: December 1, 2014

graphene sheets.[31] Among different methodologies, GO layers obtained by electrochemical reduction (erGO layers) show higher conductivities and smaller O/C ratios.[32] The main problem related to graphene-based electrochemical biosensors is their production complexity, both in the case of direct graphene deposition and when GO is used because a highly conductive electrodic interface is needed and an inefficient GO reduction drastically reduces sensor sensitivity. When an electrochemically bioactive compound, such as an enzyme, is integrated into the sensor, also a fast electronic pathway bridging the enzyme redox center and the underlying electrode is needed. This requirement does not hold for an aptamer-based biosensor where only electrodic conductivity is necessary for high performance. In summary, both electrochemical and optical graphene-based biosensors present advantages that make them versatile detection systems for accurate measurements due to high sensitivity and fast response time.[18,29] In addition, low fabrication costs can be achieved using GO as the starting material. However, they require complex validating biochemical operations that negatively affect their advantageous use.[5] Realization of an integrated optoelectrochemical sensing platform would allow obtaining both an electrochemical and an optical readout, improving sensing reliability and efficiency by (i) redundancy of detection, (ii) having internal titrations for the measurement, (iii) avoiding false positives, and (iv) internally verifying efficiency of sensor regeneration. Furthermore, an on-chip integration of this dual sensor would allow avoiding signal amplification by precise volume confinement, which increases the actual concentration of released fluorescent aptamers of some orders of magnitude and would make possible its integration within microfluidic cell culture systems as a sensing lab-on-a-chip unit. To this aim, optical transparency is highly desirable to preserve accessibility to observations of the biological systems. To achieve both optical transparency and electroconductivity, transparent indium-free conductive substrates—such as fluorine-doped tin oxide (FTO)—are particularly promising for their increased resistance to chemical corrosion and cost reduction.[33] Despite FTO surface chemical inertia, its functionalization by electrochemical grafting, controlling both the number and the type of grafted molecules, has already been reported.[34] The grafted monolayer-like film can be subsequently used as a chemical bridge for performing GO deposition.

In this work, we developed an on-chip transparent graphene-based integrated electrochemical and optical biosensing unit. A few layers of GO sheets were electrostatically immobilized on an electrochemically grafted FTO (egFTO) surface and then electrochemically reduced to achieve the required electroconductivity. In order to measure the transparency degree of the electrodes, transmittance at normal incidence was measured using a J. A. Woollam V-VASE spectroscopic ellipsometer in the wavelength range of 300−900 nm, by atomic force microscopy and scanning electron microscopy for characterizing surface topography, X-ray photoemission spectroscopy and Raman spectroscopy for characterizing the deposition steps; and cyclic voltammetry (CV) during substrate fabrication and characterization. As a proof of concept, insulin was used as the target molecule, recognized by a fluorescein-modified insulin-binding aptamer (IBA).[12] Insulin concentration in solution was indirectly measured by monitoring the adsorption of IBAs onto the electrodic surface by two integrated methods (Figure 1): (1) optically by confocal microscopy or fluorescence spectroscopy, measuring the increase of fluorescence intensity, and (2) electrochemically by electrochemical impedance spectroscopy (EIS), monitoring the increase in electrochemical impedance of a negatively charged redox probe in solution. Subnanomolar insulin optoelectrochemical detection was achieved in a microliter-volume solution.

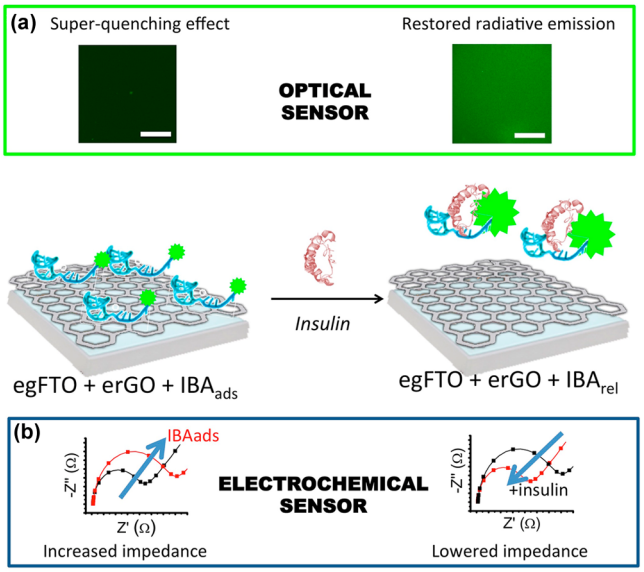

Figure 1. Schematic representation of the working principle of the graphene-based optoelectrochemical sensor. The egFTO + erGO surface is initially functionalized with fluorescein-labeled insulin-binding aptamers (IBA), whose fluorescence is quenched due to energy transfer mechanisms by the graphene layers. In parallel, the electrochemical surface impedance is measured. Once exposed to an insulin solution, the aptamer is released from the surface determining a double effect: an increase in fluorescence emission intensity (a) and a reduction in electrochemical impedance (b). Scale bar for a, 100 μm. Data points in Nyquist plots in b only represent qualitative trends.

2. EXPERIMENTAL SECTION

2.1. Substrate Preparation. All chemicals and reagents were from Sigma-Aldrich, Italy, if not differently stated. Prior to modification, FTO-coated sodalime glass (7−10 Ω/sq) was copiously rinsed with ethanol:Milli-Q-water mixture 1:1 for 15 min and then dried with nitrogen flux. Clean bare FTO electrodes were treated with UV−ozone plasma (UV/Ozone ProCleaner, BioForce Nanosciences Inc., USA), in order to maximize the number of −OH functions on FTO surfaces[34] for 20 min, followed by acetone and Milli-Q water rinsing and nitrogen dry. Clean electrodes were stored in a drybox before use.

2.2. Preparation and Characterization of Graphene Oxide. Preparation of graphene oxide (GO) was performed using a modified Hummer's method.[35,36] One gram of ultrapure graphite micrometric powder (d < 150 μm) was slowly added to 25 mL of a 9:1 mixture of concentrated H_2SO_4:H_3PO_4 (96% and 65%, respectively) in an ice−water bath. Then, 3 g of $KMnO_4$ was gradually added to the mixture under vigorous stirring. After 1 h stirring at room temperature, the mixture was heated to 35 °C for 1 h under sonication. Afterward, slow addition of 50 mL of deionized water caused an increase in temperature to about 98 °C. The mixture was maintained at this temperature for 15−20 min. The reaction ended by adding 140 mL of deionized water at 60 °C followed by 1 mL of 30% H_2O_2 solution (Fluka, Italy). After 30 min of stirring and 30 min of sonication, the yellow solid produced was collected after several cycles of centrifugation−water washing, obtaining a dispersion of GO in water with a pH of 5.5.

The obtained GO dispersion was characterized by UV−vis, Raman, and X-ray photoelectron spectroscopies (XPS). Furthermore, the Z

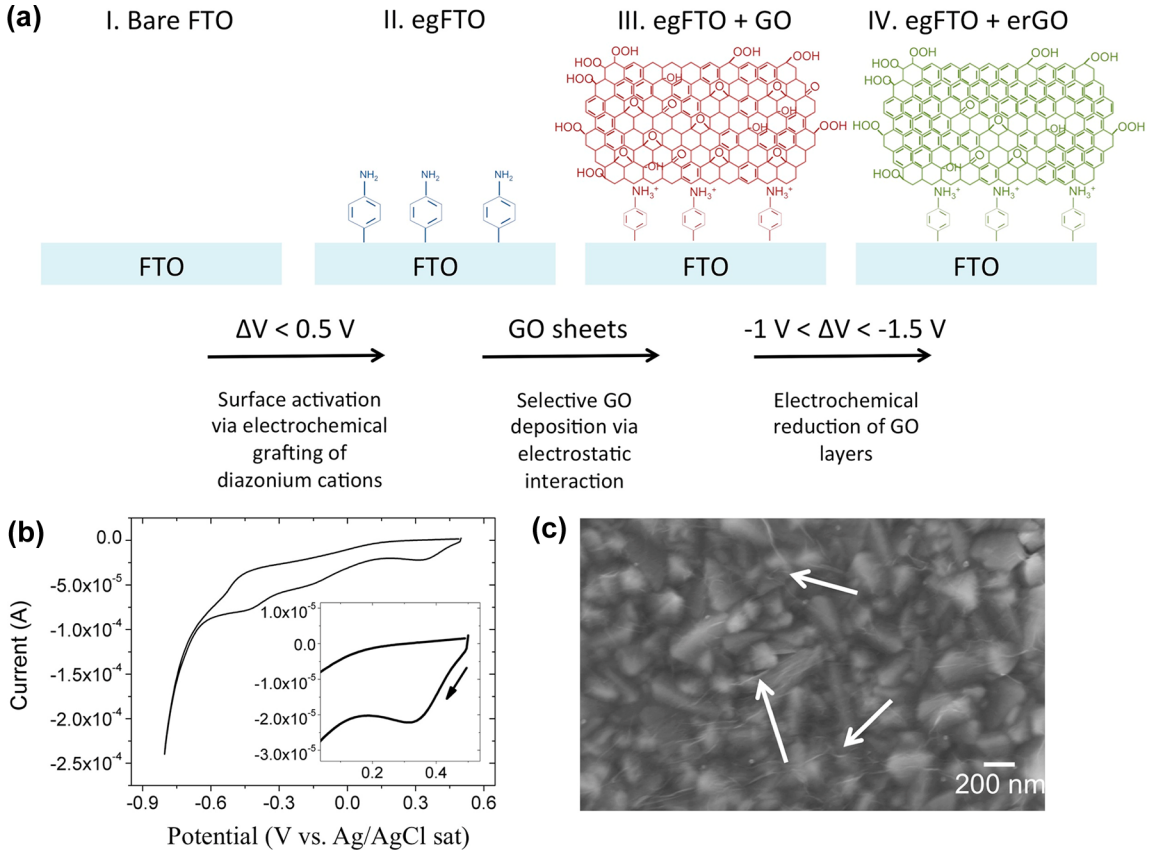

Figure 2. Fabrication of egFTO + erGO samples. (a) Schematic representation of the fabrication steps of the optoelectrochemical platform: clean FTO electrodes (Bare FTO) are covalently modified via electrochemical grafting with diazonium molecules (egFTO); then graphene oxide sheets are electrostatically bound (egFTO + GO) and finally electrochemically reduced by negative biasing (egFTO + erGO). (b) CV showing electrochemical grafting of FTO electrodes. (Inset) Enlargement of the reductive irreversible peak at 0.3 V. (c) SEM image showing few-layer deposition of graphene; arrows indicate the presence of graphene wrinkles, suggesting a graphene thin film deposition. (Inset) SEM image of a bare FTO surface. Scale bar, 600 nm.

potential of the obtained GO dispersions in water (measured by a Zetasizer (Nano-ZS), Malvern Instruments) was equal to −44.8 mV.

To characterize the lateral dimensions of the GO sheets we performed SEM measurements on different samples, prepared by means of anodic electrophoretic deposition (A-EPD) of a few layers of GO on P:Si (100) single crystal. The lateral distribution of the GO microflakes was characterized by a very high dispersion, whose sizes range from 1 to 5 μm.

2.3. Optoelectrochemical Platform Realization. The grafting solution (aryldiazonium cations solution) was prepared as follows: 5 mM $NaNO_2$ and 1 mM *p*-phenylendiamine (final concentrations) were dissolved in a 0.5 M HCl aqueous solution.[37] The latter was stirred for 5 min in the dark to guarantee formation of products and then transferred into the electrochemical cell. CV was performed for creating grafted amine layers on top of FTO surface scanning the potential cycling in the range 0.5 V: −0.9 V at −0.1 V/s. The obtained samples (egFTO samples) were vigorously washed with IPA and Milli-Q water in order to eliminate unwanted absorbed molecules and dried with nitrogen gas. Acidic water GO solution (pH = 1) was dropped onto modified FTO substrates for 18 h at room temperature in the dark. Realized egFTO + GO samples were then rinsed with Milli-Q water and dried with nitrogen. egFTO + erGO samples were fabricated by successive electrochemical reduction cycles (5 cycles) in NaCl 0.5 M at 0.1 V/s between −0.1 and −1.2 V in the negative direction. Finally, samples were rinsed with copious Milli-Q water, dried with nitrogen, and stored in a drybox when not in use.

2.4. Raman, XPS, SEM, and AFM Characterization. For Raman characterization we used a ThermoFisher DXR Raman microscope. All spectra were recorded with an excitation wavelength of 532 nm (1.5 mW), focused on the sample with a 50× objective (Olympus).

Core level photoemission spectra were taken on a VG ESCALAB MKII spectrometer using the Mg anode of a conventional non-monochromatized X-ray source ($K\alpha$ = 1253.6 eV) and with the analyzer pass energy set to 20 eV. Measurements were taken at room temperature (rt) in normal emission. The calibration of the binding energy (BE) scale was determined using Au 4f as the reference. To characterize the chemical states of carbon, the C 1s photoemission lines were separated into individual components (after Shirley background removal) using a Doniach−Sunic shape for the sp^2 component and symmetrical Voigt functions for fitting of the molecular-like C 1s components (deriving from the C−O functional groups).

The nano- and microscale characterization morphology of the materials was performed by scanning electron microscopy (SEM) using an instrument with a field emission source and equipped with a GEMINI column in a Zeiss Supra 35VP system. Micrographs have been taken with an acceleration voltage of 5 kV and using in-lens high-resolution detection.

Morphological characterization of the sample surfaces was carried out by AFM (NT-MDT, Russia) in noncontact mode. Phase images were acquired together with topology recordings to investigate the distribution of material surface characteristics.

2.5. Electrochemical Measurements. An electrochemical cell was realized using FTO electrodes as working electrodes (5 mm disk), a Pt counter electrode (Mettler Toledo, Spain), and an Ag/AgCl saturated reference electrode (Amel Instruments, Italy). Teflon tape (RS, Italy) was used for insulating electric contacts. Supporting electrolyte used for measurement was PBS 0.1 M pH 7.4 (PBS, phosphate buffer saline: 0.1 M K_2HPO_4, 0.1 M KH_2PO_4, and 0.15 M NaCl). The redox probe used was potassium ferrocyanide, 0.5 mM.

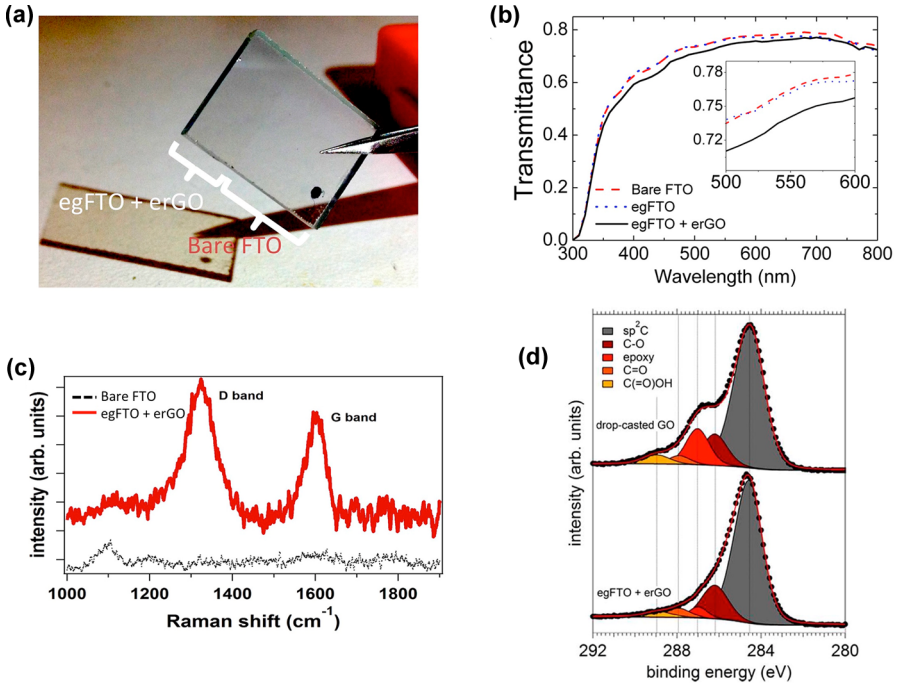

Figure 3. Characterization of Bare FTO, egFTO, and egFTO + erGO samples. (a) Picture of the samples showing the transparency of egFTO + erGO samples. (b) Transmittance spectra in the visible range acquired by an ellipsometer. (c) Raman spectra of the samples: graphene D band and G band are visible in the egFTO + erGO sample. (d) Comparison of the photoemission spectra of drop-casted GO and egFTO + erGO samples: the latter shows a diminution of oxygenated species.

The scan rate was 50 mV/s if not differently stated. Impedance measurements were recorded using a FRA2 module for frequency analyzer. Frequency scan range was established between 0.1 Hz and 100 kHz. Fitting of data was performed using NOVA software.

2.6. Confocal Microscopy Fluorescence Analysis. egFTO + IBA_{ads} samples were washed with distilled water DNase/RNase free (Life Technologies, Italy) and covered with insulin 10 g/L (about 2 mM). Images were acquired before and immediately after exposure to insulin with a Leica TCS SP5 confocal microscope (Leica, Germany). Fluorescein was excited with an argon laser at 488 nm.

2.7. Fluorescence Spectroscopy Analysis. Fluorescence spectroscopy was made with a Horiba Jobin Yvon spectrometer using a customized sample holder. For these measurements, egFTO + erGO samples were sealed to a microfluidic platform made of PMDS (polydimethylsiloxane), housing a circular reservoir of 3 mm diameter and 300 μm in height.

To promote PDMS adhesion on the functionalized surfaces avoiding any damage, only the PDMS surface was activated in a plasma cleaner for 20 min, and successively the mold was put in contact with the surface. The assembly was stored at room temperature for 24 h before use.

3. RESULTS AND DISCUSSION

3.1. Optoelectrochemical Platform Fabrication. Fabrication of the graphene-based substrate for the optoelectrochemical biosensor involved the following processes, schematically represented in Figure 2a: (I) FTO cleaning; (II) FTO modification via electrochemical grafting; (III) electrostatic immobilization of GO on grafted FTO; (IV) electrochemical reduction of bound GO sheets. All experimental details can be found in the Experimental Section.

Bare FTO samples were electrochemically modified by CV (Figure 2b). The irreversible peak at 0.3 V is related to the well-known reductive reaction involving amino groups of the aryldiazonium compounds formed in solution. Photoemission characterization confirmed covalent modification of the electrode and, on successive voltammograms, surface passivation (data not shown). This finding is similar to other results reported in the literature for analogous electrodic systems.[34,37,38]

Figure 2c shows a SEM micrograph attesting the surface modification after the end of the whole procedure. In comparison to the bare FTO sample (see inset), a quite homogeneously distributed thin layer of graphene covers the substrate, as demonstrated by its constant transparency to the electron beam. Only a few wrinkles typical of GO membrane are visible; otherwise, the erGO film is rather flat and covers in a carpeting mode the grainy texture of the substrate with just a few layers.[39,40]

This aspect is at the basis of the optical transparency of the egFTO + erGO layer, which is needed for achieving a combined optoelectrochemical detection (Figure 3a). Ellipsometry was used for quantitative determination of sample optical transparency. Specifically, the thickness of the erGO film on an egFTO-coated slide was obtained by transmittance data collected by an ellipsometer. The transmittance curves for the different samples are shown in Figure 3b. As expected, egFTO and Bare FTO curves are almost superimposable. On the other hand, the egFTO + erGO sample curve is approximately 3% lower compared to Bare FTO. Because a single layer of graphene absorbs a precise quantity of light in vacuum, given by $\pi\alpha$ = 2.3%, where α is the fine-structure constant,[41] a quasi-monolayer deposition is achieved in our system. However, GO-derived oxygen defects may alter the absorption spectra of graphene[42,43] partially affecting this film thickness estimation. Therefore, we performed a chemical analysis (XPS and Raman spectroscopy) to characterize the oxidative amount before and after the electrochemical reduction step.

Figure 3c shows Raman spectra of Bare FTO and egFTO + erGO. Both spectra have in common the band at about 1100

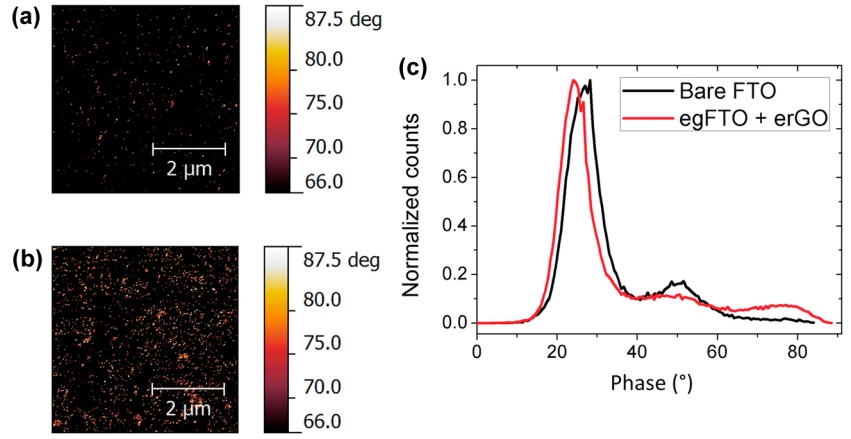

Figure 4. AFM phase images for (a) Bare FTO and (b) egFTO + erGO acquired in noncontact mode. (c) The phase distribution shows three main peaks. Bands centered at about 25° and 50° can be ascribed to the substrate, while the band present at 80° is related to the egGO-modified substrate.

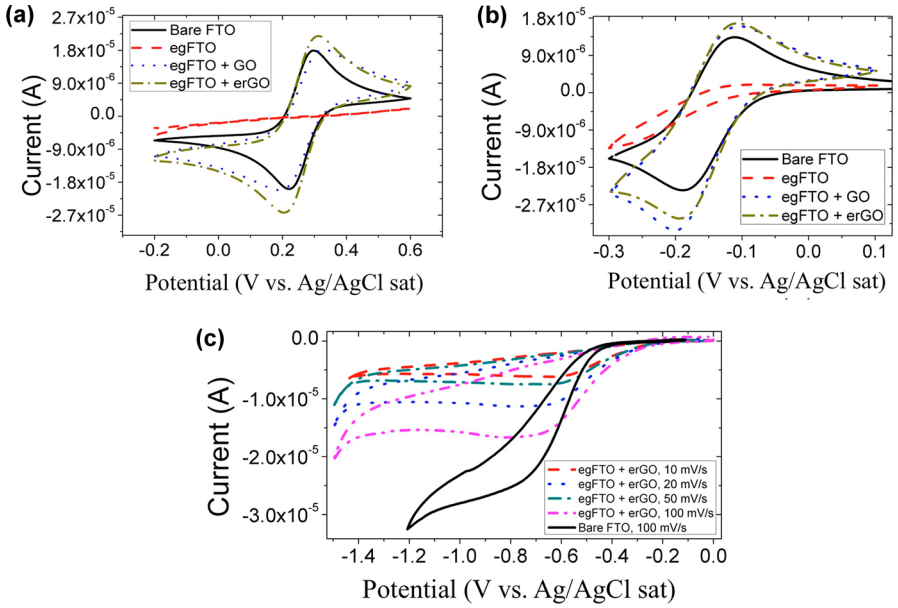

Figure 5. Electrochemical characterization. CV measurements: barrier effect toward (a) ferricyanide and (b) hexaaminеruthenium(III) for samples indicated in the legend. (c) Electrochemical window analysis for egFTO + erGO samples.

cm^{-1}, related to glass substrate Si−O stretching vibration.[44] The egFTO + erGO sample also presents the graphene D and G bands, with a D/G intensity ratio and wavenumber similar to values previously reported for reduced GO thin films obtained by other reduction techniques.[40,45,46] This result confirms the effective GO reduction by the electrochemical process and its strong immobilization on the FTO-grafted surface.

In addition, using the intensity ratio of the G band of GO to the substrate band at 1100 cm^{-1} as an indicator of the graphene layer thickness, we estimated that 1−2 layers of GO sheets are deposited, confirming the results deduced by ellipsometry measurements.

Figure 3d shows the C 1s photoemission spectra of the egFTO + erGO sample and a drop-casted GO thin film taken as reference. Multipeak analysis[47] was carried out to identify the single chemically shifted components associated with different oxygen defects. Electrochemical reduction caused an important decrease in the epoxy group content with respect to pristine GO: the epoxy group component goes from 12.7% in the pristine GO film to 3.5% in the whole C 1s peak area of the egFTO + erGO sample. This is in good agreement with the electrochemical results reported in Figure S1, Supporting Information, where an intense voltammetric peak is observed during the first cathodic scan of the electrode that can be assigned to the reduction of poorly stable epoxy species.[48]

The overall conclusion of this part is that a few layers of erGO sheets were strongly immobilized on modified FTO samples, with only a 3% diminution of transparency with respect to the bare electrode, as long as only some oxygen defects are still remaining after electrochemical reduction of GO (demonstrated in next section).

We next performed AFM analysis to verify the graphene homogeneous distribution on sample surface (Figure 4a and 4b). Topography data showed a roughness of 26 nm RMS (root mean square) for both Bare and erGO-modified FTO samples (Figure S2, Supporting Information). This result is consistent with a graphene thin film deposition, as suggested by previous SEM and transmission data. We also performed AFM phase imaging, as it is a highly sensitive tool to discriminate between areas of the sample coated by a very thin graphene

dx.doi.org/10.1021/am506941u | ACS Appl. Mater. Interfaces 2014, 6, 22769−22777

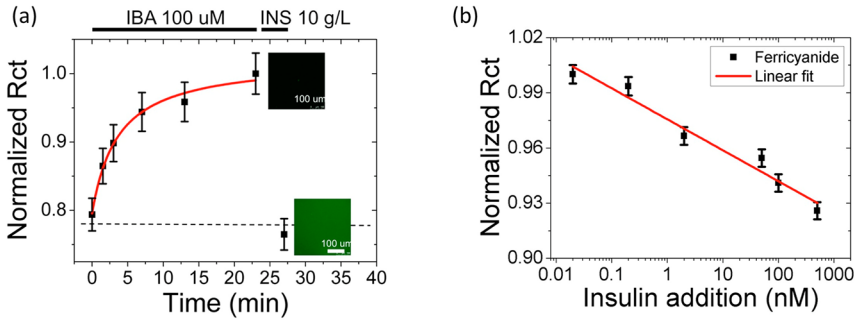

Figure 6. Electrochemical biorecognition of insulin. (a) Normalized R_{ct} value dynamics behavior shows the saturation curve of IBA adsorption on egFTO + erGO sample (experimental data fitted by red line with exponential growth curve) and electrode regeneration by insulin addition at 22 min. Error bar, standard deviation (n = 3). The horizontal dashed line refers to the egFTO + IBA_{ads} sample R_{ct} mean value. Fluorescence emission intensity before and after insulin addition is shown in the two microscope recordings reported as insets. (b) Insulin electrochemical detection in the picomolar to micromolar range using ferricyanide as redox probe.

layer and unmodified areas, even in the presence of higher roughness. The phase distribution shows three main peaks at 25°, 50°, and 80° (Figure 4c). The bands centered at about 25° and 50° can be ascribed to the substrate, with possible organic contaminations, while the band located at 80° is related to the egGO layer.

In conclusion, our electrochemical grafting strategy allowed (a) binding a few layers of GO sheets, (b) producing an optically transparent graphene-based nanocomposite platform, and (c) reducing the amount of oxygenated species compared to drop-casted samples.

3.2. Electrochemical Platform Characterization. Highly heterogeneous electron transfer kinetics for modified FTO samples produces a larger variation of impedance when aptamers are adsorbed to the surface, therefore improving biosensor sensitivity. Thus, we performed a characterization of the electrochemical performance of the biosensor starting with the study of the electrochemical barrier effect toward a redox probe in solution via CV.

Figure 5a and 5b shows the results of CVs performed in 0.1 M PBS (pH 7.4) at different stages of sensor fabrication. Two redox probes were used: ferricyanide and hexaammineruthenium(III), which are negatively and positively charged, respectively. In the first case, the curve associated with the bare FTO sample showed high electron transfer rates, with a quasi-reversible behavior and an approximately 100 mV difference between faradic peaks. No current was observed after the electrode was modified with arylamine molecules (egFTO sample), whereas a restored electron transfer was achieved after GO was covalently bound to the electrode. However, a less reversible behavior was established (i.e., a peak separation of about 150 mV) in egFTO + GO sample, probably due to the presence of oxygenated species in the GO sheets that reduce electron mobility in the C sp^2 domains. This result is in contrast with Wang's work,[23] where a glassy carbon electrode was modified with silanes, but in fair agreement with the recent work of Haque and co-workers,[49] where GO was electrochemically grafted to ITO surfaces. After electrochemical reduction of GO, the charge transfer kinetics became comparable to that of Bare FTO samples and the current was increased. This result demonstrates that (a) most of the oxygenated species were successfully removed during the electrochemically reducing step, (b) the transparent graphene film grafted on top of the FTO surface is highly conductive, (c) the last reductive step is necessary for the surface to be used as a highly performing electrochemical sensing system.

CV measurements were also performed with hexamminoruthenium(III) to study the charge effect of the redox probe in the electrochemical behavior (Figure 5b). No variations were noticed in the trend of the blocking effect with respect to negatively charged redox probe voltammetric analysis (Figure 5a). This result demonstrates that the barrier effect on redox probes diffusion is due to steric hindrance and not only to electrostatic repulsion, confirming a close-packed distribution of grafted molecules on FTO surface. Thus, either positive or negative redox probes can be successfully used to characterize biosensor electrochemical measurements.

Defining the effective potential window that can be used for measurements is important to avoid contemporary undesired reactions. In Figure 5c CVs of egFTO + erGO samples at different scan rates were compared (solid lines), whereas Bare FTO sample at 100 mV/s is shown for reference (dotted line). FTO glasses have a complex cathodic behavior due to metal ion reduction that falls approximately below −0.4 V in PBS 1X. Also, hydrogen starts to be produced at −1.2 V. The egFTO + erGO electrode exhibits a wider electrochemical stability window with respect to bare FTO (Figure 5c). In the former system, hydrogen evolution is shifted toward a more cathodic potential (almost 300 mV). Therefore, the egFTO + erGO system constitutes a suitable electrochemical platform for detecting complex molecules having biological relevance (such as proteins or FAD), since it is a stable and inert electrode characterized by the absence of undesired reactions (such hydrogen evolution) on a wide potential range.

3.3. Optoelectrochemical Biorecognition. We performed the optoelectrochemical biorecognition of a biologically relevant protein, insulin, which is involved in glucose metabolism regulation and related to a severe disease such as diabetes.[50] As shown in Figure 1, the sensing element that confers selectivity to the measurement is a fluorescein-modified IBA, initially adsorbed on the electrode surface.

First, we studied the kinetics of physical adsorption of IBA onto the egFTO + erGO sample via EIS (Figure 6a).

The modified Randles equivalent circuit (Figure S3, Supporting Information) was used, including R_s, the constant-phase element CPE, the Warburg impedance (W), and the charge-transfer resistance (R_{ct}). In particular, the R_s value depends on the solution conductivity, while W module results from the redox probe diffusion through the surface layer. The CPE instead of the ideal capacitance, C_{dl}, was used to better account for the capacitive behavior of the double-layer and the diffusion contribution.[51] R_{ct}, which models interfacial electron

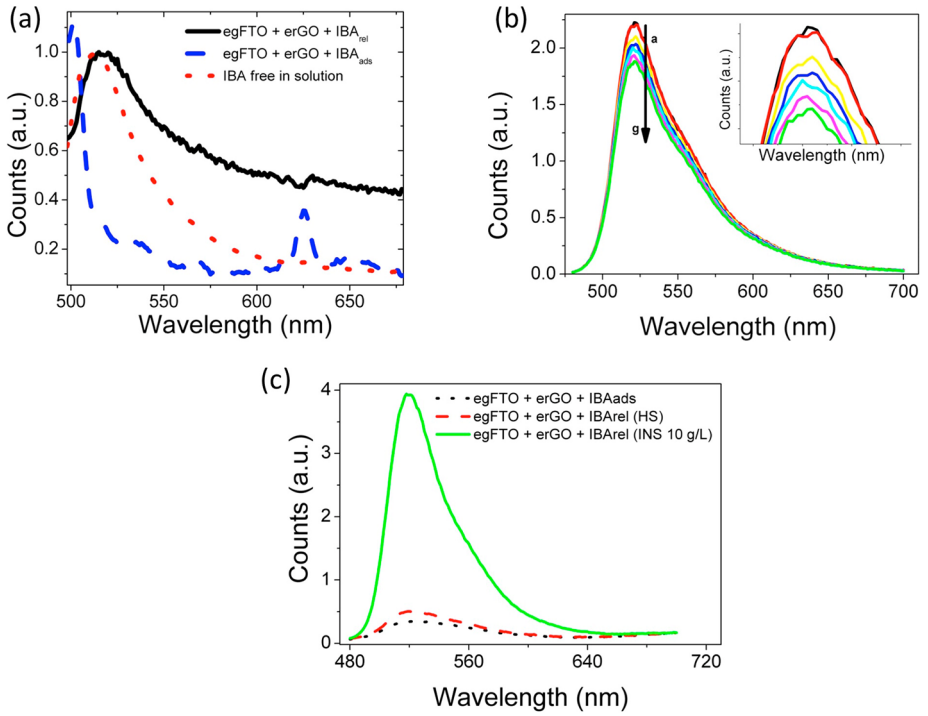

Figure 7. Optical biorecognition of insulin performed by fluorescence spectroscopy within a microfluidic platform. (a) Emission spectrum for IBA free in solution, adsorbed on egFTO + erGO, and detached from the sample surface at an insulin concentration of 2 mM. (b) Monitoring of IBA adsorption on egFTO + erGO as a function of time: 0 (a), 1 (b), 5 (c), 10 (d), 15 (e), 20 (f), and 30 min (g). (c) Sensor optical response in terms of fluorescence emission to horse serum and 2 mM insulin addition. Control was given by a phosphate buffer saline solution.

transfer kinetics between the redox probe and the electrode surface, was considered as a function of IBA adsorption. R_{ct} increased for longer IBA immersion times, as measurements were performed with a negatively charged redox probe, ferricyanide. The progressive increment of R_{ct} value was due to the electrostatic repulsion between the negatively charged IBA-modified surface and ferricyanide.[52] The contrary would occur if a positively charged redox probe was used (data not shown). From data in Figure 5a, the immersion time required to saturate the surface by the aptamer (calculated as 95% of the R_{ct} plateau value) was approximately 20 min. We verified that the sensor could be fully regenerated by adding in solution a large amount of insulin (2 mM), which restores the initial R_{ct} value with no aptamer adsorbed on the surface (Figure 6a).

Release of IBA from the surface, as a consequence of insulin binding, was also qualitatively followed by measuring the restored fluorescence emission (Figure 6a) through an analysis performed by confocal fluorescence microscopy. For our system, the quenching yield of the egFTO + erGO surface was about 80% (Figure S4, Supporting Information).

Starting from an electrode saturated with the aptamer (egFTO + erGO + IBA$_{ads}$ sample), we performed a calibration curve of the insulin sensor by EIS using a ferrocyanide redox probe (Figure 6b). As expected, the R_{ct} value decreased at increasing insulin concentrations, because a negatively charged probe was used. The response was linear in the concentration range of 0.01−500 nM, and a sensitivity of 17 pM^{-1} was calculated as the slope of the linear regression line. The actual lowest measured concentration is 0.01 nM, a value at least 1 order of magnitude lower than that in other similar systems that do not include amplification.[12]

In order to enhance interface phenomena, the active optoelectrochemical protein biosensor was integrated in a microfluidic environment. Given a microfluidic channel height of 100 μm and an IBA surface coverage of about 1 nmol/cm^2 the insulin-dependent IBA detachment from the surface produces its accumulation in solution in the microfluidic confined environment, with a concentration that can reach some millimolar. Moreover, use of a customized microfluidic platform allows regenerating the biosensor simply and rapidly to perform multiple successive measurements for continuous monitoring. In Figure 7a emission spectra for different samples within the microfluidic platform are shown. For optical quantitative detection of insulin the fluorescence emission spectra of IBA before and after full detachment (after insulin addition) from the egFTO + erGO sample surface are shown. As expected, fluorescence emission intensity increased when IBA was detached from the surface. The peak position shift in the aptamer emission spectrum compared to the emission peak of the reference free IBA in solution could be attributed to insulin modifying the electronic energy levels of the fluorophore when binding IBA.

Figure 7b and 7c shows the fluorescence spectra of the sensor integrated in the microfluidic system. First, IBA adsorption on egFTO + erGO surface was monitored (Figure 7b). Consistent with the results from the electrochemical data, surface saturation was achieved in approximately 25 min. Figure 7c shows the sensor optical response in terms of fluorescence emission to horse serum and to a 2 mM insulin addition (recorded 5 min after addition). Horse serum insulin concentration is generally unknown and lot dependent. We detected the presence of a small amount of insulin in the horse serum used, producing a slight increase of the emission band centered at 525 nm. Addition of a 2 mM final insulin concentration resulted in a strong sensor response.

Altogether these results showed that (a) egFTO samples are actually accessible to optical analyses, (b) GO/erGO modification does not alter the optical transparency if only few layers are immobilized, and (c) highly sensitive biosensors can be realized using graphene as a sensing platform within microfluidic channels.

4. CONCLUSIONS

In this work we showed a new experimental strategy for protein biorecognition involving combined electrochemical and optical measurements based on graphene-specific properties. Deep morphological, chemical, and electrochemical characterization demonstrated the peculiar features of this optoelectrochemical platform. In particular, to the best of our knowledge, this is the first work obtaining the same graphene-modified substrate for biorecognition having both high electron transfer rates and optical accessibility. Previously, for high conductivity, a thick graphene film had to be deposited, compromising optical transparency. On the other hand, the most used substrates for fabricating thin-layer graphene-based optically transparent sensors were glasses or inert transparent materials with limited electron mobility. We achieved an effective robust modification of an optically transparent electrode substrate with high-conductance graphene. Specifically, we were able to immobilize a few layers of electrochemically reduced graphene oxide sheets via electrostatic linkage on an electrochemically grafted FTO surface. This strategy allowed fabrication of a graphene-based optoelectrochemical sensor able to detect insulin, used as a test target molecule, at subnanomolar concentrations in a few-microliter volume solution within microfluidic channels. Therefore, FTO and graphene were successfully coupled to develop a high-performance low-cost regenerable protein sensor for biological applications.

■ ASSOCIATED CONTENT

Supporting Information

Voltammetric, AFM, and fluorescence data. This material is available free of charge via the Internet at http://pubs.acs.org.

■ AUTHOR INFORMATION

Corresponding Author

*E-mail: nicola.elvassore@unipd.it.

Author Contributions

F.L. performed electrochemical and optoelectrochemical experiments. L.B. performed ellipsometric, AFM, and optical measurements. M.F. produced the graphene oxide sheets. A.Z. performed confocal measurements. S.A., M.F., M.C., and G.G. performed XPS, Raman, and SEM measurements and relative analyses. F.L. and C.L. designed the insulin biosensor. G.B. actively collaborated during the discussion of surface characterization. F.L., L.B., M.G., C.L., and N.E. wrote the manuscript. F.L, M.G., and N.E. conceived and designed the experiments.

Notes

The authors declare no competing financial interest.

■ ACKNOWLEDGMENTS

Dr. Lidia Armelao and Dr. Gregorio Bottaro, Department of Chemical Sciences and CNR, University of Padova, are gratefully acknowledged for the collaboration in collecting fluorescence spectroscopy data. F.L. was supported by a University of Padova grant. The authors acknowledge funding from Italian Ministry for University and Research (MIUR). M.F. acknowledges Fondazione Cariparo for financial support. S.A., G.G., M.F., and M.C. acknowledges the Italian MIUR national grant Futuro in Ricerca 2012 RBFR128BEC "Beyond graphene: tailored C-layers for novel catalytic materials and green chemistry" and the University of Padova for funding project CPDA128318/12, "Study of the catalytic activity of complex graphene nanoarchitectures from ideal to real conditions".

■ REFERENCES

(1) Arlett, J. L.; Myers, E. B.; Roukes, M. L. Comparative Advantages of Mechanical Biosensors. *Nat. Nanotechnol.* **2011**, *6*, 203−215.

(2) Han, M.; Gao, X.; Su, J. Z.; Nie, S. Quantum-Dot-Tagged Microbeads for Multiplexed Optical Coding of Biomolecules. *Nat. Biotechnol.* **2001**, *19*, 631−635.

(3) Yang, W.; Ratinac, K. R.; Ringer, S. P.; Thordarson, P.; Gooding, J. J.; Braet, F. Carbon Nanomaterials in Biosensors: Should You Use Nanotubes or Graphene? *Angew. Chem., Int. Ed.* **2010**, *49*, 2114−2138.

(4) Vollmer, F.; Arnold, S. Whispering-Gallery-Mode Biosensing: Label-free Detection Down to Single Molecules. *Nat. Methods* **2008**, *5*, 591−596.

(5) Ma, H.; Wu, D.; Cui, Z.; Li, Y.; Zhang, Y.; Du, B.; Wei, Q. Graphene-Based Optical and Electrochemical Biosensors: A Review. *Anal. Lett.* **2013**, *46*, 1−17.

(6) Tang, Z.; Wu, H.; Cort, J. R.; Buchko, G. W.; Zhang, Y.; Shao, Y.; Aksay, I. A.; Liu, J.; Lin, Y. Constraint of DNA on Functionalized Graphene Improves its Biostability and Specificity. *Small* **2010**, *6*, 1205−1209.

(7) Wang, Y.; Li, Z.; Wang, J.; Li, J.; Lin, Y. Graphene and Graphene Oxide: Biofunctionalization and Applications in Biotechnology. *Trends Biotechnol.* **2011**, *29*, 205−212.

(8) Wang, Y.; Li, Z.; Hu, D.; Lin, C.; Li, J.; Lin, Y. Aptamer/Graphene Oxide Nanocomplex for In Situ Molecular Probing in Living Cells. *J. Am. Chem. Soc.* **2010**, *132*, 9274−9276.

(9) Kimoto, M.; Yamashige, R.; Matsunaga, K.; Yokoyama, S.; Hirao, I. Generation of High-Affinity DNA Aptamers Using an Expanded Genetic Alphabet. *Nat. Biotechnol.* **2013**, *31*, 453−457.

(10) Wu, C.; Zhou, Y.; Miao, X.; Ling, L. A Novel Fluorescent Biosensor for Sequence-Specific Recognition of Double-stranded DNA with the Platform of Graphene Oxide. *Analyst* **2011**, *136*, 2106−2110.

(11) Chang, H.; Tang, L.; Wang, Y.; Jiang, J.; Li, J. Graphene Fluorescence Resonance Energy Transfer Aptasensor for the Thrombin Detection. *Anal. Chem.* **2010**, *82*, 2341−2346.

(12) Pu, Y.; Zhu, Z.; Han, D.; Liu, H.; Liu, J.; Liao, J.; Zhang, K.; Tan, W. Insulin-Binding Aptamer-Conjugated Graphene Oxide for Insulin Detection. *Analyst* **2011**, *136*, 4138−4140.

(13) Sheng, L.; Ren, J.; Miao, Y.; Wang, J.; Wang, E. PVP-coated Graphene Oxide for Selective Determination of Ochratoxin A via Quenching Fluorescence of Free Aptamer. *Biosens. Bioelectron.* **2011**, *26*, 3494−3499.

(14) Dong, H.; Gao, W.; Yan, F.; Ji, H.; Ju, H. Fluorescence Resonance Energy Transfer Between Quantum Dots and Graphene Oxide for Sensing Biomolecules. *Anal. Chem.* **2010**, *82*, 5511−5517.

(15) Balapanuru, J.; Yang, J.; Xiao, S.; Bao, Q.; Jahan, M.; Polavarapu, L.; Wei, J.; Xu, Q.; Loh, K. P. A Graphene Oxide−Organic Dye Ionic Complex with DNA-Sensing and Optical-Limiting Properties. *Angew. Chem., Int. Ed.* **2010**, *122*, 6699−6703.

(16) Lu, C.; Yang, H.; Zhu, C.; Chen, X.; Chen, G. A Graphene Platform for Sensing Biomolecules. *Angew. Chem., Int. Ed.* **2009**, *121*, 4879−4881.

(17) He, S.; Song, B.; Li, D.; Zhu, C.; Qi, W.; Wen, Y.; Wang, L.; Song, S.; Fang, H.; Fan, C. A Graphene Nanoprobe for Rapid, Sensitive, and Multicolor Fluorescent DNA Analysis. *Adv. Funct. Mater.* **2010**, *20*, 453−459.

(18) Loh, K. P.; Bao, Q.; Eda, G.; Chhowalla, M. Graphene Oxide as a Chemically Tunable Platform for Optical Applications. *Nat. Chem.* **2010**, *2*, 1015−1024.

(19) He, S.; Song, B.; Li, D.; Zhu, C.; Qi, W.; Wen, Y.; Wang, L.; Song, S.; Fang, H.; Fan, C. A Graphene Nanoprobe for Rapid, Sensitive, and Multicolor Fluorescent DNA Analysis. *Adv. Funct. Mater.* **2010**, *20*, 453−459.
(20) Lu, Z.; Zhang, L.; Deng, Y.; Li, S.; He, N. Graphene Oxide for Rapid MicroRNA Detection. *Nanoscale* **2012**, *4*, 5840−5842.
(21) Lin, W.; Liao, C.; Jhang, J.; Tsai, Y. Graphene Modified Basal and Edge Plane Pyrolytic Graphite Electrodes for Electrocatalytic Oxidation of Hydrogen Peroxide and β-Nicotinamide Adenine Dinucleotide. *Electrochem. Commun.* **2009**, *11*, 2153−2156.
(22) Shan, C.; Yang, H.; Han, D.; Zhang, Q.; Ivaska, A.; Niu, L. Graphene/AuNPs/Chitosan Nanocomposites Film for Glucose Biosensing. *Biosens. Bioelectron.* **2010**, *25*, 1070−1074.
(23) Wang, Z.; Zhou, X.; Zhang, J.; Boey, F.; Zhang, H. Direct Electrochemical Reduction of Single-layer Graphene Oxide and Subsequent Functionalization with Glucose Oxidase. *J. Phys. Chem. C* **2009**, *113*, 14071−14075.
(24) Kang, X.; Wang, J.; Wu, H.; Aksay, I. A.; Liu, J.; Lin, Y. Glucose Oxidase−Graphene−Chitosan Modified Electrode for Direct Electrochemistry and Glucose Sensing. *Biosens. Bioelectron.* **2009**, *25*, 901−905.
(25) Lu, J.; Drzal, L. T.; Worden, R. M.; Lee, I. Simple Fabrication of a Highly Sensitive Glucose Biosensor Using Enzymes Immobilized in Exfoliated Graphite Nanoplatelets Nafion Membrane. *Chem. Mater.* **2007**, *19*, 6240−6246.
(26) Reina, A.; Jia, X.; Ho, J.; Nezich, D.; Son, H.; Bulovic, V.; Dresselhaus, M. S.; Kong, J. Large Area, Few-layer Graphene Films on Arbitrary Substrates by Chemical Vapor Deposition. *Nano Lett.* **2008**, *9*, 30−35.
(27) Kim, K. S.; Zhao, Y.; Jang, H.; Lee, S. Y.; Kim, J. M.; Kim, K. S.; Ahn, J.; Kim, P.; Choi, J.; Hong, B. H. Large-scale Pattern Growth of Graphene Films for Stretchable Transparent Electrodes. *Nature* **2009**, *457*, 706−710.
(28) Shan, C.; Yang, H.; Song, J.; Han, D.; Ivaska, A.; Niu, L. Direct Electrochemistry of Glucose Oxidase and Biosensing for Glucose Based on Graphene. *Anal. Chem.* **2009**, *81*, 2378−2382.
(29) Shao, Y.; Wang, J.; Wu, H.; Liu, J.; Aksay, I. A.; Lin, Y. Graphene Based Electrochemical Sensors and Biosensors: a Review. *Electroanal.* **2010**, *22*, 1027−1036.
(30) Pumera, M.; Ambrosi, A.; Bonanni, A.; Chng, E. L. K.; Poh, H. L. Graphene for Electrochemical Sensing and Biosensing. *TrAC, Trends Anal. Chem.* **2010**, *29*, 954−965.
(31) Dreyer, D. R.; Park, S.; Bielawski, C. W.; Ruoff, R. S. The Chemistry of Graphene Oxide. *Chem. Soc. Rev.* **2010**, *39*, 228−240.
(32) Du, M.; Yang, T.; Jiao, K. Immobilization-free Direct Electrochemical Detection for DNA Specific Sequences Based on Electrochemically Converted Gold Nanoparticles/Graphene Composite Film. *J. Mater. Chem.* **2010**, *20*, 9253−9260.
(33) Minami, T. Substitution of Transparent Conducting Oxide Thin Films for Indium Tin Oxide Transparent Electrode Applications. *Thin Solid Films* **2008**, *516*, 1314−1321.
(34) Lamberti, F.; Agnoli, S.; Brigo, L.; Granozzi, G.; Giomo, M.; Elvassore, N. Surface Functionalization of Fluorine-doped Tin Oxide Samples Through Electrochemical Grafting. *ACS Appl. Mater. Interfaces* **2013**, *5*, 12887.
(35) Hummers, W. S., Jr.; Offeman, R. E. Preparation of Graphitic Oxide. *J. Am. Chem. Soc.* **1958**, *80*, 1339−1339.
(36) Marcano, D. C.; Kosynkin, D. V.; Berlin, J. M.; Sinitskii, A.; Sun, Z.; Slesarev, A.; Alemany, L. B.; Lu, W.; Tour, J. M. Improved Synthesis of Graphene Oxide. *ACS Nano* **2010**, *4*, 4806−4814.
(37) Tasca, F.; Ludwig, R.; Gorton, L.; Antiochia, R. Determination of Lactose by a Novel Third Generation Biosensor Based on a Cellobiose Dehydrogenase and Aryl Diazonium Modified Single Wall Carbon Nanotubes Electrode. *Sens. Actuators, B: Chem.* **2013**, *177*, 64−69.
(38) Mahouche-Chergui, S.; Gam-Derouich, S.; Mangeney, C.; Chehimi, M. M. Aryl Diazonium Salts: a New Class of Coupling Agents for Bonding Polymers, Biomacromolecules and Nanoparticles to Surfaces. *Chem. Soc. Rev.* **2011**, *40*, 4143−4166.
(39) Dikin, D. A.; Stankovich, S.; Zimney, E. J.; Piner, R. D.; Dommett, G. H.; Evmenenko, G.; Nguyen, S. T.; Ruoff, R. S. Preparation and Characterization of Graphene Oxide Paper. *Nature* **2007**, *448*, 457−460.
(40) Favaro, M.; Agnoli, S.; Di Valentin, C.; Mattevi, C.; Cattelan, M.; Artiglia, L.; Magnano, E.; Bondino, F.; Nappini, S.; Granozzi, G. TiO_2/Graphene Nanocomposites from the Direct Reduction of Graphene Oxide by Metal Evaporation. *Carbon* **2014**, *68*, 319−329.
(41) Kuzmenko, A.; Van Heumen, E.; Carbone, F.; Van Der Marel, D. Universal Optical Conductance of Graphite. *Phys. Rev. Lett.* **2008**, *100*, 117401.
(42) Eda, G.; Fanchini, G.; Chhowalla, M. Large-area Ultrathin Films of Reduced Graphene Oxide as a Transparent and Flexible Electronic Material. *Nat. Nanotechnol.* **2008**, *3*, 270−274.
(43) Zhao, J.; Pei, S.; Ren, W.; Gao, L.; Cheng, H. Efficient Preparation of Large-area Graphene Oxide Sheets for Transparent Conductive Films. *ACS Nano* **2010**, *4*, 5245−5252.
(44) Chrimes, A. F.; Khoshmanesh, K.; Stoddart, P. R.; Mitchell, A.; Kalantar-zadeh, K. Microfluidics and Raman Microscopy: Current Applications and Future Challenges. *Chem. Soc. Rev.* **2013**, *42*, 5880−5906.
(45) Wang, Z.; Wu, S.; Zhang, J.; Chen, P.; Yang, G.; Zhou, X.; Zhang, Q.; Yan, Q.; Zhang, H. Comparative Studies on Single-layer Reduced Graphene Oxide Films Obtained by Electrochemical Reduction and Hydrazine Vapor Reduction. *Nanoscale Res. Lett.* **2012**, *7*, 1−7.
(46) Ramesha, G. K.; Sampath, S. Electrochemical Reduction of Oriented Graphene Oxide Films: an In Situ Raman Spectroelectrochemical Study. *J. Phys. Chem. C* **2009**, *113*, 7985−7989.
(47) Favaro, M.; Agnoli, S.; Cattelan, M.; Moretto, A.; Durante, C.; Leonardi, S.; Kunze-Liebhäuser, J.; Schneider, O.; Gennaro, A.; Granozzi, G. Shaping Graphene Oxide by Electrochemistry: from Foams to Self-Assembled Molecular Materials. *Carbon* **2014**, *77*, 405.
(48) Toh, H. S.; Ambrosi, A.; Chua, C. K.; Pumera, M. Graphene Oxides Exhibit Limited Cathodic Potential Window Due to Their Inherent Electroactivity. *J. Phys. Chem. C* **2011**, *115*, 17647−17650.
(49) Haque, A. J.; Park, H.; Sung, D.; Jon, S.; Choi, S.; Kim, K. An Electrochemically Reduced Graphene Oxide-based Electrochemical Immunosensing Platform for Ultrasensitive Antigen Detection. *Anal. Chem.* **2012**, *84*, 1871−1878.
(50) Alberti, K. G.; Mayer, M.; Zimmet, P. Z. Definition, Diagnosis and Classification of Diabetes Mellitus and its Complications. Part 1: Diagnosis and Classification of Diabetes Mellitus. Provisional Report of a WHO Consultation. *Diabetic Med.* **1998**, *15*, 539−553.
(51) Lamberti, F.; Ferraro, D.; Giomo, M.; Elvassore, N. Enhancement of Heterogeneous Electron Transfer Dynamics Tuning Single-Walled Carbon Nanotube Forest Height and Density. *Electrochim. Acta* **2013**, *97*, 304−312.
(52) Rodriguez, M. C.; Kawde, A.; Wang, J. Aptamer Biosensor for label-free Impedance Spectroscopy Detection of Proteins Based on Recognition-induced Switching of the Surface Charge. *Chem. Commun.* **2005**, *34*, 4267−4269.